Prepared for submission to JCAP

# Interacting warm dark matter

**Norman Cruz,**[a] **Guillermo Palma,**[a] **David Zambrano**[a] **and Arturo Avelino**[b]

[a]Departamento de Física, Facultad de Ciencia,
Universidad de Santiago de Chile,
Casilla 307, Santiago, Chile.
[b]Departamento de Física, DCI, Campus León,
Universidad de Guanajuato,
CP. 37150, León, Guanajuato, México.

E-mail: norman.cruz@usach.cl

**Abstract.** We explore a cosmological model composed by a dark matter fluid interacting with a dark energy fluid. The interaction term has the non-linear $\lambda\rho_{\rm m}^{\alpha}\rho_{\rm e}^{\beta}$ form, where $\rho_m$ and $\rho_e$ are the energy densities of the dark matter and dark energy, respectively. The parameters $\alpha$ and $\beta$ in principle are not constraint to take any particular values. We perform an analytical study of the evolution equations, finding the fixed points and their stability properties in order to characterize suitable physical regions in the space of the dark matter and dark energy densities. The constants $(\lambda, \alpha, \beta)$ as well as $(w_{\rm m}, w_{\rm e})$ of the EoS of dark matter and dark energy respectively were estimated using the cosmological observations of the type Ia supernovae data set and the Hubble parameter $H(z)$ at different redshift. We found that the best fit to data is for a model with a phantom dark energy interacting with a warm dark matter, where the energy transfer comes from the dark energy to the dark matter and with an interacting term of the simple form "$\rho_{\rm m}\rho_{\rm e}$". This result is consistent with stable solutions of the dynamical system analysis.

**Keywords:** Interacting model, phantom dark energy, warm dark matter

## Contents



## 1 Introduction

The existence of a dark component with an exotic equation of state, i. e., with a ratio $w = p/\rho$ negative and close to $-1$, which drives an accelerated expansion, is consistent with data coming from Supernovae Ia (SNe Ia) [1], large scale structure formation (LSS) [2], cosmic microwave background radiation (CMB) [3], baryon acoustic oscillations (BAO) [4] and weak lensing [5].

Cosmic observations show that densities of dark energy (DE) and dark matter (DM) are of the same order today, despite their different decreasing rates. To solve this coincidence problem [6] an evolving dark energy field with a non-gravitational interaction with matter [7] is assumed (decay of dark energy to dark matter). In this case both dark fluids interact via an additional coupling term in the fluid equations. In the current research different forms of coupling have been considered. Most of them study the coupling between cold DM and DE. In general, the interactions investigated are particular cases the form $\lambda_m H\rho_m + \lambda_e H\rho_e$, where $H$ is the Hubble parameter, and $\rho_m$ and $\rho_e$ are the dark matter and dark energy densities respectively. Nevertheless, non linear interactions of the form $\lambda\frac{\rho_m\rho_e}{\rho_m+\rho_e}$ were considered in [8]. A more plausible interaction is inspired by the situation of two types of fluids interacting, where the interaction is proportional to the product of the powers of the number density of both components. In this case the interaction rate goes to zero as one or both densities become zero, and increase with each of the densities. We then consider in this paper an interaction of the form $\lambda\rho_m^\alpha\rho_e^\beta$, where the parameter $\lambda$ has dimensions of $[density^{\alpha+\beta-1} \times time]^{-1}$. This type of interaction was investigated in the framework of an holographic dark energy [9] and in

coupled quintessence [10], where the evolution of the energy densities of the dark interacting components was investigated for different values of the parameters $\alpha$ and $\beta$. A cyclic scenario for the present situation $\rho_e \sim \rho_m$ was found as a possible solution to the coincidence problem. The particular case $\alpha = \beta = 1$ was studied in [11]. In this case if the energy is transferred from dark energy to dark matter ($\lambda > 0$), and for a dark energy of a phantom type ($w_e < -1$) the energy densities also presents periodic orbits. A general result, which is independent of the interaction type, and only assumes that the energy is transferred from dark energy to dark matter, pointed out that stationary solutions of the ratio $r = \rho_m/\rho_e$ require a phantom dark energy [12].

The aim of this paper is to study the time evolution of the dark sector densities when the above mentioned interaction is considered. This evolution is driven by a highly non-linear coupled differential equations when the parameters $\alpha$ and $\beta$ are let free. We solve numerically these equations and also study analytically the stability of the fixed-points. Since has been argued that second law of thermodynamics and Le Châtelier's principle implies $\lambda > 0$ [13] we do not consider here the case of energy transferred from dark matter to dark energy.

In most of the investigation which take into account this type of non lineal interaction, cold dark matter with zero pressure is taken to be interacting with the dark energy fluid. Nevertheless, current research has opened the possibility that a warm dark matter component fits better new results found at the level of galaxies and cluster of galaxies [14]. For a wide discussion on this matter see [15]. In this work we investigate how a warm dark matter modifies the behavior of an interacting dark sector and the constraints for its EoS (assuming a barotropic form) derived from astrophysical observations.

Our paper is organized as follows. In section II we present the effective equations of state for the interacting dark components, assuming that the energy is transferred from dark energy to dark matter. We also extend the result found in [12] in order to find the condition for stationary points of the parameter $r$ when the dark matter is assumed not to be dust. In section III we study the two coupled differential equations corresponding to continuity equations of both interacting fluids. We study analytically the fixed-points including their stability. In section IV, we obtain numerical solutions using a numerical method of adaptive step-size algorithm called Bulirsch-Stoer method. We explore the behavior of the fixed points varying the parameters $\alpha$, $\beta$ and the EoS of both dark sector components.

We study the stationary solutions and their stability for the equations of evolution of the ratios between the DM and DE and the third fluid and DE. We present the constraints on the equations of state for DE and the hypothetical third fluid. In section IV we discuss our results. Section V is an Appendix in which the conditions for the stability of the stationary solutions, corresponding to the three different couplings, are discussed.

## 2 General considerations of an interacting dark sector

In the following we assume a flat FRW universe filled basically with the fluids of the dark sector. We consider a warm dark matter of density $\rho_m$ and a dark energy component described by the density $\rho_e$. For simplicity we also assume that both fluids obey a barotropic EoS, so we have $p_m = w_m \rho_m$, for the warm dark matter and $p_e = w_e \rho_e$ for dark energy. In what follows we restrict our model to the late time of cosmic evolution, which implies that the others components of the universe, like radiation and baryons are negligible. In this case the sourced Friedmann equation is given by

$$3H^2 = \rho_m + \rho_e, \tag{2.1}$$

where $8\pi G = 1$ has been adopted. We will assume that the dark matter component is interacting with the dark energy component, so their continuity equations take the form

$$\dot{\rho}_m + 3(1+w_m)H\rho_m = +Q \tag{2.2}$$

$$\dot{\rho}_e + 3(1+w_e)H\rho_e = -Q, \tag{2.3}$$

where $H = \dot{a}/a$ is the Hubble parameter, and $a(t)$ is the scale-factor. Here, an overdot indicates a time derivative. $Q$ represents the interaction term, despite that we do not use a specific functional dependence at this stage, we will only assume that $Q$ do not change its sign during the cosmic evolution.

### 2.1 Effective EoS for interacting fluids

Let us discuss briefly the behavior of the dark components in terms of an effective EoS driven by the interacting term. Rewriting the continuity equation (2.2) in the usual form

$$\dot{\rho}_m + 3(1+w_{m_{eff}})H\rho_m = 0, \tag{2.4}$$

where $w_{m_{eff}}$ represents the effective EoS for the interacting dark matter, which is given by

$$w_{m_{eff}} = w_m - \frac{Q}{3H\rho_m}. \tag{2.5}$$

Note that the behavior of $w_{m_{eff}}$ can be quite different if $w_m$ is non zero. With the usual assumption of cold dark matter ($w_m = 0$) and $Q > 0$, which implies that energy is transferred from dark energy to dark matter, some kind of exotic dark matter with a negative EoS is driven, assuming, of course, that we are in an expanding universe $H > 0$. For warm dark matter we would have, depending on the type of interaction considered and the strength of the coupling constant appearing in $Q$, a possible change of the sign on the effective EoS during the cosmic evolution. For the dark energy, the effective EoS is given by

$$w_{\Lambda_{eff}} = w_e + \frac{Q}{3H\rho_e}. \tag{2.6}$$

For $Q > 0$ the above equation indicates, even for $w_e = -1$ (cosmological constant), that the effective Dark Energy (DE) fluid will behave as a quintessence field. Then, an effective phantom behavior can only be obtained if $w_e < -1$.

### 2.2 The behavior of the coincidence parameter parameter $r$

In order to address the coincidence problem, in terms of the dynamics of the parameter $r \equiv \rho_m/\rho_e$, we will make in what follows a similar analysis along the line describes in ref. [12]. The dynamics of the parameter $r$ is given by

$$\dot{r} = r\left(\frac{\dot{\rho_m}}{\rho_m} - \frac{\dot{\rho_e}}{\rho_e}\right), \tag{2.7}$$

where the dot indicates derivative with respect to the cosmic time. Changing the time derivatives by a derivative with respect to $\ln a^3$ which will be denoted by a prime, i.e. $\dot{\rho} = \rho' 3H$, eqs (2.2) and (2.3) go into

$$\frac{\rho_m'}{\rho_m} = -(1+w_m) + \frac{Q}{3H\rho_m}, \quad \frac{\rho_e'}{\rho_e} = -(1+w_e) - \frac{Q}{3H\rho_e}. \tag{2.8}$$

In terms of total density $\rho = \rho_e + \rho_m$, we obtain

$$\rho' = -\left[1 + \frac{w_m r + w_e}{r+1}\right]\rho. \tag{2.9}$$

For the coincidence parameter $r$ the evolution equation reads

$$r' = r\left[(w_m + w_e) + \frac{Q}{3H}\frac{(1+r)^2}{r\rho}\right]. \tag{2.10}$$

Before specifying any particular type of interaction, we will discuss some general of these equations. The critical point of Eq. (2.9) is given by

$$r_c = -\frac{(1+w_e)}{w_m+1}. \tag{2.11}$$

If $w_m > 0$ (warm dark matter) and since $r$ must be positive, it follows that $w_e < -1$, which corresponds to a phantom DE. Using the condition $r' = 0$ in Eq.(2.10) and the value of $r_c$ one finds

$$\rho_c = -\frac{(w_m - w_e)}{w_m+1}\ \frac{Q}{3H(1+w_e)}. \tag{2.12}$$

Depending on the value of $w_m$ three cases can be analyze.

### 2.3 Case $w_m = 0$

In this case, Eq. (2.12) simplifies to

$$\rho_c = \frac{w_e}{w_m+1}\ \frac{Q}{3H}. \tag{2.13}$$

This case was analyzed in [12], concluding that a positive stationary energy density $\rho_c$ requires $Q > 0$ since $w_e < -1$. This means that independent on the interaction type, the existence of critical points require a positive exchange from dark energy to dark matter (DM).

### 2.4 Case $w_m > 0$ (warm dark matter)

For this case the expression for $\rho_c$ becomes

$$\rho_c = \frac{w_e - w_m}{w_m+1}\frac{Q}{3H(1+w_e)}. \tag{2.14}$$

The condition $w_e < -1$ leads in this case to same result found in 2.3 for the sign of $Q$. This result also holds for $-1 < w_m < 0$.

We find here the general condition to have accelerated expansion in terms of the energy densities of the dark components and their EoS. Differentiating (2.1) with respect to $t$ and substituting for $\dot{\rho}_m$ and $\dot{\rho}_e$ gives the auxiliary equation

$$2\dot{H} = -(1+w_m)\rho_m - (1+w_e)\rho_e. \tag{2.15}$$

The acceleration is given by the relation $\ddot{a} = a(\dot{H} + H^2)$. From (2.1) and (2.15), we have

$$\ddot{a} = -\frac{a}{6}(\rho_m(1+3w_m) + (1+3w_e)\rho_e). \tag{2.16}$$

The condition $\ddot{a} > 0$ leads to the condition

$$\rho_e > -\frac{1+3w_m}{1+3w_e}\rho_m. \tag{2.17}$$

Since we shall consider $w_e < -1$ this condition represent a right line with positive slope $1 + 3w_m/3|w_e| - 1$ in the plane $(\rho_m, \rho_e)$.

## 3 Evolution equations: Fixed points and stability analysis

Introducing the interaction term $Q = \lambda\rho_m^\alpha\rho_e^\beta$ in Eqs. (2.2) and (2.3) yields

$$\dot{\rho}_m = -3(1+w_m)H\rho_m + \lambda\rho_m^\alpha\rho_e^\beta \tag{3.1}$$
$$\dot{\rho}_e = -3(1+w_e)H\rho_e - \lambda\rho_m^\alpha\rho_e^\beta. \tag{3.2}$$

The time evolution of the dark matter and dark energy densities is given by the highly non-linear coupled differential equations (3.1) and (3.2). We rewrite them as follows:

$$\dot{\rho}_i = f_i(\rho_m, \rho_e), \tag{3.3}$$

where $i = m, e$. The functions $f_m$ and $f_e$ are defined by the following expressions

$$f_m(\rho_m, \rho_e) = -\sqrt{3}\,(1+w_m)\,\rho_m\,(\rho_m+\rho_e)^{1/2} + \lambda\rho_m^\alpha\rho_e^\beta \tag{3.4}$$
$$f_e(\rho_m, \rho_e) = -\sqrt{3}\,(1+w_e)\,\rho_e\,(\rho_m+\rho_e)^{1/2} - \lambda\rho_m^\alpha\rho_e^\beta. \tag{3.5}$$

From numerical results we expect that the above equations have some non-trivial fixed-points $(\bar{\rho}_m, \bar{\rho}_e)$, which we want to study analytically including their stability properties. In spite of the non-linearities and according to ref. [16], it is still possible to analyze the stability of fixed points by using the linearized piece of the original differential equations

$$\dot{\rho}_i = \sum_j a_{ij}\rho_j + R_i(\rho_m, \rho_e) \tag{3.6}$$

provided the inequality

$$|R_i(\rho_m, \rho_e)| \leq N\left(\sum_i \rho_i^2\right)^{\frac{1}{2}+\alpha} \tag{3.7}$$

is fulfilled in a neighbor region around the fixed points.

To achieve this goal we expand both the dark matter and dark energy densities around their fixed point values $(\bar{\rho}_m, \bar{\rho}_e)$ as follows:

$$\rho_m^\alpha = (\bar{\rho}_m + \mu\rho_m)^\alpha = \bar{\rho}_m{}^\alpha + \alpha\mu\rho_m + \mathcal{O}\left(\mu^2\rho_m^2/\bar{\rho}_m\right)$$
$$\rho_e^\beta = (\bar{\rho}_e + \mu\rho_e)^\beta = \bar{\rho}_e{}^\beta + \beta\mu\rho_e + \mathcal{O}\left(\mu^2\rho_e^2/\bar{\rho}_e\right),$$

it also holds

$$(\rho_m+\rho_e)^{1/2} = \left(\bar{\rho}_m{}^\alpha + \bar{\rho}_e{}^\beta\right)^{1/2} + \frac{1}{2\left(\bar{\rho}_m{}^\alpha + \bar{\rho}_e{}^\beta\right)^{1/2}}\mu\,(\rho_m+\rho_e) + \mathcal{O}\left(\mu^2\right).$$

Inserting the above perturbative expressions into the differential equation system one obtains up to first order in $\mu$:

$$\dot{\rho}_i = \sum_j a_{ij}\rho_j \tag{3.8}$$

or explicitly

$$\dot{\rho}_m = -\sqrt{3}\,(1+\omega_m)\left[\frac{\bar{\rho}_m\,(\rho_m+\rho_e)}{2\,(\bar{\rho}_m+\bar{\rho}_e)^{1/2}} + \rho_m\,(\bar{\rho}_m+\bar{\rho}_e)^{1/2}\right] + \lambda\left[\beta\rho_e\bar{\rho}_m{}^{\alpha} + \alpha\rho_m\bar{\rho}_e{}^{\beta}\right] \tag{3.9}$$

$$\dot{\rho}_e = -\sqrt{3}\,(1+\omega_e)\left[\frac{\bar{\rho}_e\,(\rho_m+\rho_e)}{2\,(\bar{\rho}_m+\bar{\rho}_e)^{1/2}} + \rho_e\,(\bar{\rho}_m+\bar{\rho}_e)^{1/2}\right] - \lambda\left[\beta\rho_e\bar{\rho}_m{}^{\alpha} + \alpha\rho_m\bar{\rho}_e{}^{\beta}\right]. \tag{3.10}$$

The tree level values are implicitly defined by the relations

$$\sqrt{3}\,(1+w_m)\,\bar{\rho}_m\,(\bar{\rho}_m+\bar{\rho}_e)^{1/2} = \lambda\bar{\rho}_m{}^{\alpha}\bar{\rho}_e{}^{\beta} \tag{3.11}$$

$$\sqrt{3}\,(1+w_e)\,\bar{\rho}_e\,(\bar{\rho}_m+\bar{\rho}_e)^{1/2} = -\lambda\bar{\rho}_m{}^{\alpha}\bar{\rho}_e{}^{\beta}, \tag{3.12}$$

or equivalently,

$$\bar{\rho}_e = -\frac{1+\omega_m}{1+\omega_e}\bar{\rho_m} \tag{3.13}$$

$$\bar{\rho}_m = \left[(-1)^{\beta}\frac{\lambda}{\sqrt{3}}\frac{(1+\omega_m)^{\beta-1}(1+\omega_e)^{1/2-\beta}}{(\omega_e-\omega_m)^{1/2}}\right]^{(3/2-\alpha-\beta)^{-1}}. \tag{3.14}$$

Now we are prepared to analyze the different numerical results obtained from the direct numerical solution of the system of eqs. (3.3). The numerical solutions were obtained by using a very accurate numerical method of adaptive step-size algorithm called Bulirsch–Stoer method, which will be explained in the next section.

We will use the numerical values $\omega_m = 0$ and $\omega_e = -1.1$, which are of physical interest as we will discuss it in the next section. For these particular values, the above equations have a fixed point given by $\bar{\rho}_e = 10\bar{\rho}_m$ and

$$\bar{\rho_m} = \left(\frac{\lambda}{1+\omega_m}\frac{10^{\beta}}{\sqrt{33}}\right)^{(3/2-\alpha-\beta)^{-1}} \tag{3.15}$$

These fixed points are displayed in figures 3 and 4, and their loci agree remarkably well with the corresponding ones of the numerical results.

In particular, for $\alpha = 0.9$, $\beta = 1.0$, $\omega_m = 0$ and $\lambda = 1$, eq. (3.15) leads to the relation $\bar{\rho}_m \approx 0.25$, which is in agreement with the corresponding locus shown in figure 4. For the next attractor, $\alpha = 0.8$, $\beta = 1.0$, $\omega_m = 0$ and $\lambda = 1$, eq (3.15) gives $\bar{\rho}_m \approx 0.16$, which again perfectly agreed with the numerical result shown in figure 4.

Now we comeback to the linearized system of eqs. (3.9) and (3.10). We rewrite it explicitly as the homogeneous system of differential equations

$$\dot{\rho}_m = \left(-\sqrt{(3)}\,(1+\omega_m)\left[\frac{\bar{\rho}_m}{2\,(\bar{\rho}_m+\bar{\rho}_e)^{1/2}}+(\bar{\rho}_m+\bar{\rho}_e)^{1/2}\right]+\lambda\alpha\bar{\rho}_e{}^{\beta}\right)\rho_m + \left(-\sqrt{(3)}\,(1+\omega_m)\left[\frac{\bar{\rho}_m}{2\,(\bar{\rho}_m+\bar{\rho}_e)^{1/2}}\right]+\lambda\beta\bar{\rho}_m{}^{\alpha}\right)\rho_e \tag{3.16}$$

$$\dot{\rho}_e = \left(-\sqrt{(3)}\,(1+\omega_e)\left[\frac{\bar{\rho}_e}{2\,(\bar{\rho}_m+\bar{\rho}_e)^{1/2}}+(\bar{\rho}_m+\bar{\rho}_e)^{1/2}\right]-\lambda\beta\bar{\rho}_m{}^{\alpha}\right)\rho_e + \left(-\sqrt{(3)}\,(1+\omega_e)\left[\frac{\bar{\rho}_e}{2\,(\bar{\rho}_m+\bar{\rho}_e)^{1/2}}\right]-\lambda\alpha\bar{\rho}_e{}^{\beta}\right)\rho_m. \tag{3.17}$$

The stability of the fixed points of the above equations depend on the eigenvalues given by characteristic equation associated to the system:

$$k^2-(a_{11}+a_{22})\,k+(a_{11}a_{22}-a_{12}a_{12})=0. \tag{3.18}$$

As it is well known, depending on the roots of eq. (3.18), the trajectories around the fixed-point ($\tilde{\rho}_m=0$, $\tilde{\rho}_e=0$) will be stable or unstable, (see for instance [16]).

For example, if all roots of the characteristic eq. (3.18) have negative real parts, then the trivial solution $(\rho_m\ \ \rho_e)^T=(0\ \ 0)^T$ of the linearized system and of the non-linear system (3.3) is asymptotically stable. On the other side, if at least one of the roots of eq. (3.18) has a positive real part then both systems have an unstable fixed point at $(0\ \ 0)^T$.

For the interacting model described by eq. (3.3), there are five physical parameters, $w_m$, $w_e$, $\lambda$, $\alpha$ and $\beta$, which should be chosen according to both, physical stability properties on one side, and compatibility with observational data on the other side. The solutions of eq. (3.18) were numerically evaluated for different regions of the parameter space, and found the interesting physical region defined by the inequalities: $0\leq\omega_m\leq 1/3$, $-2-\omega_m<\omega_e<-1$, $\lambda>1$, $0.0155<\alpha<0.222$ and $0.59<\alpha<1.02$ for $\omega_m=0$ and $\beta>0.8$. From it, we will considered the subregion $0\leq\omega_m\leq 1/3$, $\omega_e=-1.1$, $\lambda=1$, $\alpha=0.9$ and $\beta=1$. In particular, in these regions the condition 3.7 holds, which guaranties that the linear analysis of stability also apply to the non-linear differential equation considered.

## 4 Numerical analysis

In this section we present numerical results obtained by using the Bulirsch–Stoer method to solve the non-linear coupled system of eqs. (3.3). The Bulirsch–Stoer method uses an adaptive step-size control parameter, which ensures extremely high accuracy with comparatively little extra computational effort. In the past, this method has proven to be very accurate for solving non-linear differential equations [17]. In addition, we have computed the fixed point trajectories for different values of the five physical parameters $w_m$, $w_e$, $\lambda$, $\alpha$ and $\beta$. The corresponding trajectories within the stability region discussed in the previous section, will be shown in the figures bellow.

The evolution of matter an energy densities $\rho_m$ and $\rho_e$ depends critically on the value of the parameter $w_e$. In particular, for $w_e>-1$, the system exhibits a smooth evolution of the densities towards the fixed point. On the other side, if $w_e<-1$ the system shows periodic

orbits around the fixed point. In this case, a slight variation of the exponents $\alpha$ and $\beta$ leads to spiral orbits as it is shown in figures 3 and 4.

### 4.1 Symmetry for $w_e$ and $w_m$

We will now consider the particular values $\alpha = \beta = 1$, which has been claimed to give the best fit to observations [9] for an interaction term of the form $\lambda\rho_m^\alpha\rho_e^\beta$. As explained above, we have used the Bulirsch–Stoer method to solve numerically 3.3.

For $\lambda = 1$, $0 < w_m < 1/3$ and $-1.0 < w_e < -1.1$ the trajectories of the matter and energy densities are displayed in the figures below. For the fixed value $w_m = 0$ and $w_e$ within the interval $[-1.1, -1.0]$, different trajectories are shown in figure 1, which have the remarkable feature of having two intersection points. These points are characterized by the same value of $\rho_m = 0.4$. For the fixed value $w_e = -1.1$ and $w_m$ within the interval $[0, 1/3]$, different trajectories are shown in figure 2. In this case the intersection points arise at the same value of $\rho_e = 3.5$.

In both cases the fixed points are of center point type, with the exception of $w_m = 0$ and $w_e = -1$, which corresponds to a crossover value (see figure 1).

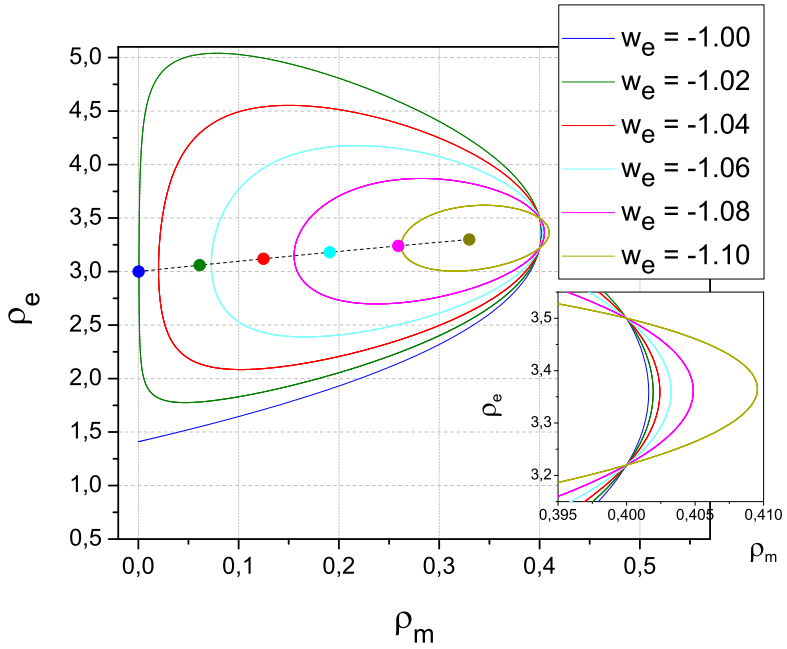


**Figure 1**. (Color on-line) For the parameters $\alpha = \beta = \lambda = 1$, $w_m = 0$ and $w_e = [-1.0, \ -1, 1]$ different evolutions of the densities are shown starting from the same initial values. Two intersection points can be identify for the same value of $\rho_m$ when the range of $w_e$ is swept. The dots represent the fixed points given by eq. (3.13) and (3.14).

### 4.2 Spiral trajectories

From the previous subsection, closed trajectories are obtained only for the region defined by $w_e < -1$. Depending on the values of $\alpha$ and $\beta$, converging or diverging spirals are obtained. In fact, $\alpha < 1$ and $\beta > 1$ lead to convergent spirals and $\alpha > 1$ and $\beta < 1$ lead to divergent spirals (see figures 3 and 4).

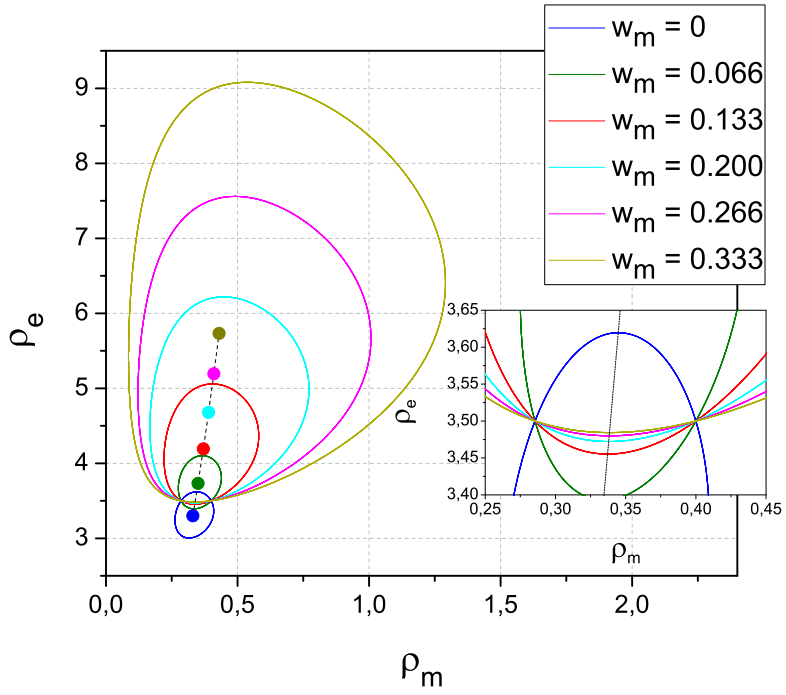


**Figure 2**. (Color on-line) For the parameters $\alpha = \beta = \lambda = 1$, $w_e = -1.1$ and $w_m = [0, \ -1/3]$ different evolutions of the densities are shown starting from the same initial values. Two intersection points can be identify for the same value of $\rho_e$ when the range of $w_m$ is swept. The dots represent the fixed points given by eq. (3.13) and (3.14).

## 5 Observational Constraints

### 5.1 The Hubble parameter

In a spatially flat FRW Universe, the Hubble constraint and the conservation equations for the matter and dark energy fluids are given as

$$H^2 = \frac{8\pi G}{3}(\rho_{\rm m} + \rho_{\rm e}), \tag{5.1}$$

$$\dot{\rho}_{\rm m} + 3H(\rho_{\rm m} + p_{\rm m}) = \lambda \rho_{\rm m}^{\alpha} \rho_{\rm e}^{\beta}, \tag{5.2}$$

$$\dot{\rho}_{\rm e} + 3H(\rho_{\rm e} + p_{\rm e}) = -\lambda \rho_{\rm m}^{\alpha} \rho_{\rm e}^{\beta}, \tag{5.3}$$

where $H$ is the Hubble parameter and $\lambda$ is a constant to quantify the strength of the interaction between the matter with the dark energy. These equations can be written in terms of the scale factor $a$ as

$$\frac{d\rho_{\rm m}}{da} + \frac{3}{a}\rho_{\rm m}(1 + w_{\rm m}) = \frac{\lambda\, \rho_{\rm m}^{\alpha} \rho_{\rm e}^{\beta}}{aH}, \tag{5.4a}$$

$$\frac{d\rho_{\rm e}}{da} + \frac{3}{a}\rho_{\rm e}(1 + w_{\rm e}) = -\frac{\lambda\, \rho_{\rm m}^{\alpha} \rho_{\rm e}^{\beta}}{aH}. \tag{5.4b}$$

We define the dimensionless parameter $\bar{\lambda}$ related with $\lambda$ as

$$\lambda = \frac{\bar{\lambda}\, H_0}{(\rho_{\rm crit}^0)^{\alpha-1} (\rho_{\rm crit}^0)^{\beta}}, \tag{5.5}$$

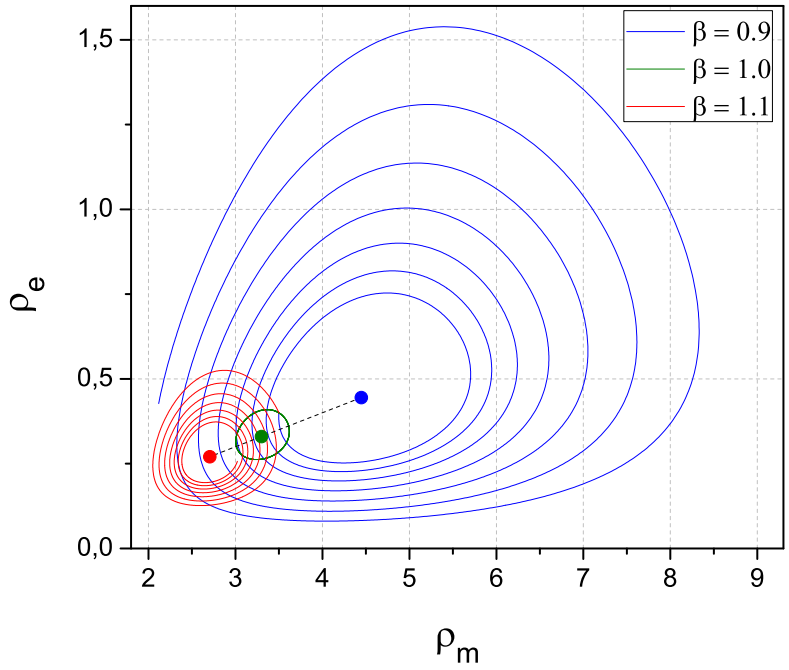


**Figure 3**. (Color on-line) For initial values $\rho_m = 0.4$ and $\rho_e = 3.5$ and for the parameters $\alpha = \beta = \lambda = 1$, $w_m = 0$ and $w_e = -1.1$, a close orbit is shown –blue line– around its fixed point –blue dot–. Starting for the same initial values but changing the value of the exponents *beta*, spiral trajectories are shown for the evolution of the densities –red and green lines–, for $\beta = 0.9$ the evolution moves away from the fixed points while for $\beta = 1.1$ the evolution is towards the fixed point.

where $\rho^0_{\rm crit} \equiv 3H_0^2/(8\pi G)$ is the *critical density* evaluated today and $H_0$ is the Hubble constant. We define also the dimensionless parameter density $\hat{\Omega}_i \equiv \rho_i/\rho^0_{\rm crit}$ with $i = m, e$. Using these definitions, the Friedmann constraint equation (5.1) can be expressed as $H = H_0\sqrt{\hat{\Omega}_{\rm m} + \hat{\Omega}_{\rm e}}$, and the conservation eqs. (5.4) become

$$\frac{d\hat{\Omega}_{\rm m}}{da} + \frac{3}{a}\hat{\Omega}_{\rm m}(1 + w_{\rm m}) = \bar{\lambda}\,\frac{\hat{\Omega}_{\rm m}^{\alpha}\,\hat{\Omega}_{\rm e}^{\beta}}{a\sqrt{\hat{\Omega}_{\rm m} + \hat{\Omega}_{\rm e}}}, \tag{5.6a}$$

$$\frac{d\hat{\Omega}_{\rm e}}{da} + \frac{3}{a}\hat{\Omega}_{\rm e}(1 + w_{\rm e}) = -\bar{\lambda}\,\frac{\hat{\Omega}_{\rm m}^{\alpha}\,\hat{\Omega}_{\rm e}^{\beta}}{a\sqrt{\hat{\Omega}_{\rm m} + \hat{\Omega}_{\rm e}}}. \tag{5.6b}$$

Using the relation between the scale factor and the redshift $z$ given by $a = 1/(1+z)$ we express eqs. (5.6) in terms of the redshift as

$$\frac{d\hat{\Omega}_{\rm m}}{dz} = \frac{1}{1+z}\left[3(1 + w_{\rm m})\hat{\Omega}_{\rm m} - \bar{\lambda}\frac{\hat{\Omega}_{\rm m}^{\alpha}\,\hat{\Omega}_{\rm e}^{\beta}}{\sqrt{\hat{\Omega}_{\rm m} + \hat{\Omega}_{\rm e}}}\right], \tag{5.7a}$$

$$\frac{d\hat{\Omega}_{\rm e}}{dz} = \frac{1}{1+z}\left[3(1 + w_{\rm e})\hat{\Omega}_{\rm e} + \bar{\lambda}\frac{\hat{\Omega}_{\rm m}^{\alpha}\,\hat{\Omega}_{\rm e}^{\beta}}{\sqrt{\hat{\Omega}_{\rm m} + \hat{\Omega}_{\rm e}}}\right]. \tag{5.7b}$$

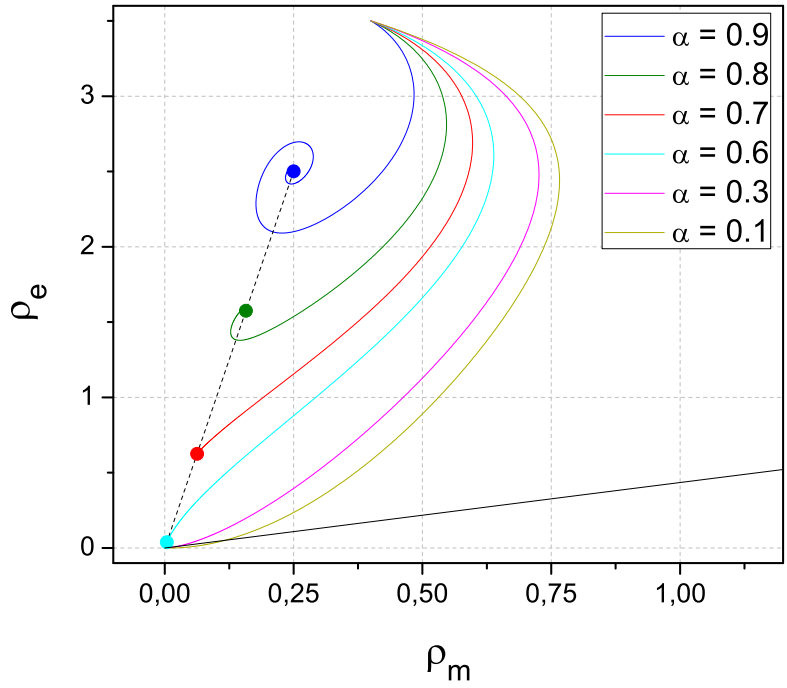


**Figure 4**. (Color on-line) Phase diagrams for $\rho_m$ and $\rho_e$ (starting from the same initial conditions) are given by the color lines for different values of $\alpha$, and for $\lambda = \beta = 1$, $w_m = 0$ and $w_e = -1.1$. They were obtain by solving numerically eqs. (3.4) and (3.5). For this figure and all the following ones, the black dashed line represent the fixed-point trajectory given in eqs. (3.13) and (3.14). The full black line is the zero-acceleration line given by the expression (2.15) with $\ddot{a} = 0$, the region above this line correspond to an accelerating universe while the region below this line correspond to a deceleration universe.

We solve numerically this ordinary differential equation system (ODEs) for the functions $\hat{\Omega}_{\rm m}(z)$ and $\hat{\Omega}_{\rm e}(z)$, with the initial conditions $\hat{\Omega}_{\rm m}(z=0) \equiv \Omega_{\rm m0} = 0.274$, and $\hat{\Omega}_{\rm e}(z=0) \equiv \Omega_{\rm e0} = 0.726$.

The dimensionless Hubble parameter $E \equiv H/H_0$ becomes

$$E(z, \alpha, \beta, \bar{\lambda}, w_{\rm m}, w_{\rm e}) = \sqrt{\hat{\Omega}_{\rm m}(z) + \hat{\Omega}_{\rm e}(z)}, \tag{5.8}$$

where $\hat{\Omega}_{\rm m}(z)$ and $\hat{\Omega}_{\rm e}(z)$ are given by the solution of the ODEs (5.7).

### 5.2 Cosmological probes

We constrain the values of the free parameters $(\alpha, \beta, \bar{\lambda}, w_{\rm m}, w_{\rm e})$ using the cosmological observations that measure the expansion history of the Universe explained in the following sections. We compute the best estimated value for each parameter through a minimizing process of a $\chi^2$ function defined below, and calculate their probability density functions (or likelihood function).

#### 5.2.1 Type Ia Supernovae

We use the type Ia supernovae (SNe Ia) of the "Union2.1" data set (2012) from the Supernova Cosmology Project (SCP) composed of 580 SNe Ia [18]. The luminosity distance $d_L$ in a spatially flat FRW Universe is defined as

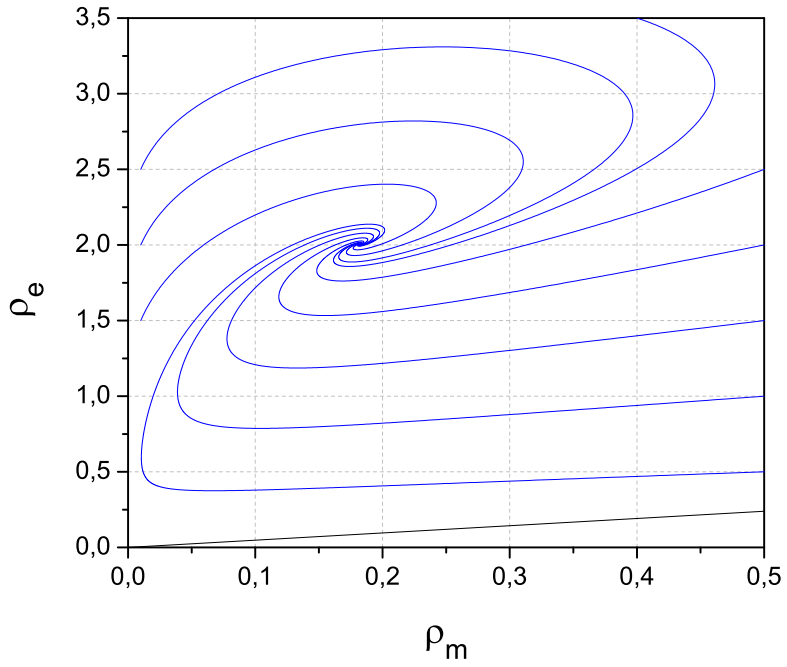


**Figure 5**. (Color on-line) Phase diagrams for the parameters $\alpha = 0.8$, $\lambda = \beta = 1$, $w_m = 0.1$ and $w_e = -1.1$. Spiral evolution of the densities towards the fixed points is shown.

| | | | Assumptions | | | | |
|---|---|---|---|---|---|---|---|
| Best estimate | $\chi^2_{\rm d.o.f.}$ | $\chi^2$ | $\bar{\lambda}$ | $\alpha$ | $\beta$ | $w_{\rm m}$ | $w_{\rm e}$ |
| $\bar{\lambda} = 1.497 \pm 0.24$ | 1.30 | 773.62 | – | 0.9 | 1 | 0 | $-1$ |
| $\bar{\lambda} = 2.257 \pm 0.18$ | 1.29 | 762.78 | – | 0.9 | 1 | 0.2 | $-1.1$ |
| $\alpha = 0.379^{+0.11}_{-0.10}$ | 1.29 | 767.46 | 1 | – | 1 | 0 | $-1$ |
| $\alpha = 0.30^{+0.09}_{-0.08}$ | 1.23 | 732.96 | 1 | – | 1 | 0.1 | $-1.1$ |
| $\beta = 1.171 \pm 0.8$ | 1.22 | 722.89 | 1 | 0.9 | – | 0 | $-1.1$ |
| $w_{\rm m} = -0.062 \pm 0.028$ | 1.21 | 718.37 | 1 | 1 | 1 | – | $-1.1$ |
| $w_{\rm e} = -1.288 \pm 0.03$ | 1.14 | 684.48 | 1 | 1 | 1 | 0 | – |
| $w_{\rm e} = -1.416 \pm 0.03$ | 1.10 | 658.23 | 1 | 1 | 1 | 0.1 | – |

**Table 1**. Best estimated values for $(\bar{\lambda}, \alpha, \beta, w_{\rm m}, w_{\rm e})$ (left column) assuming some particular values indicates at the last five columns. The best estimates where computed using the joint SNe+$H(z)$ data sets. See section 5.2 for details. The likelihood functions for each estimated parameter are shown in figures 7 to 14, as well as the stable regions of the critical points of the dynamical system analysis. From the value of $\chi^2_{\rm d.o.f.}$ seen as measure of the goodness-of-fit to data we find that the best fit to the cosmological observations corresponds to the bottom row of the table where $\chi^2_{\rm d.o.f.} = 1.10$, i.e., a model of a phantom dark energy ($w_{\rm e} = -1.4$) interacting with a warm dark matter ($w_{\rm m} = 0.1$), where the energy transfer comes from the dark energy to the dark matter ($\bar{\lambda} = 1$) and with an interacting term with the simple form "$\rho_{\rm m}\rho_{\rm e}$". The errors correspond to $1\sigma$ (68.3%) of confidence level.

$$d_L(z) = \frac{c(1+z)}{H_0} \int_0^z \frac{dz'}{E(z')} \tag{5.9}$$

where $E(z)$ corresponds to the expression (5.8), and "$c$" corresponds to the speed of light in

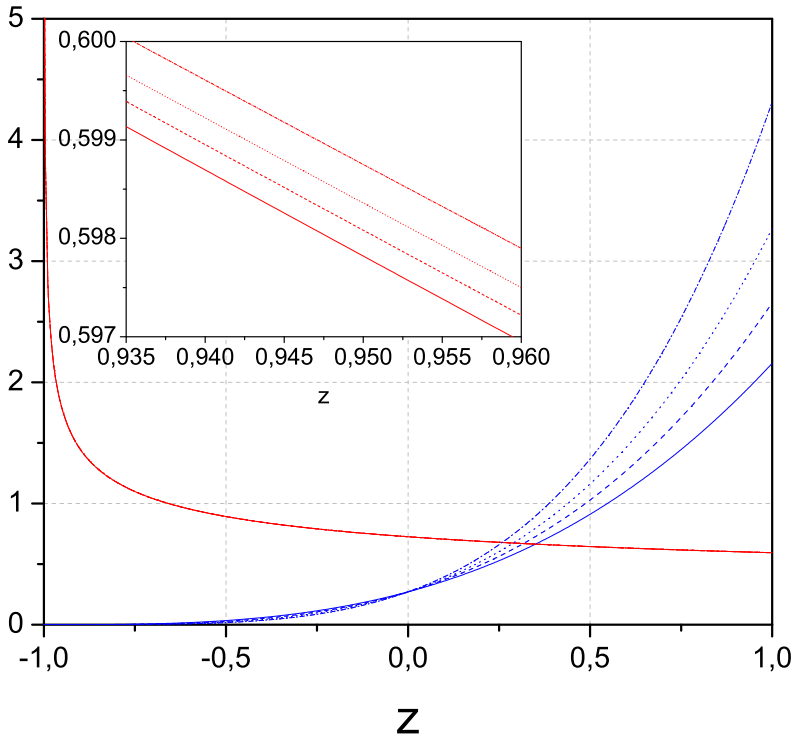


**Figure 6**. (Color on-line) Evolution for $\hat{\Omega}_{\rm m}(z)$ (blue) and $\hat{\Omega}_{\rm e}(z)$ (red), with the initial conditions $\hat{\Omega}_{\rm m}(z=0) \equiv \Omega_{\rm m0} = 0.274$ and $\hat{\Omega}_{\rm e}(z=0) \equiv \Omega_{\rm e0} = 0.726$ (present time $z = 0$). The parameters are $\alpha = 0.9$, $\beta = 1$ and $w_e = -1.1$. Full lines are for $w_m = 0.0$, dashed lines are for $w_m = 0.1$, doted lines are for $w_m = 0.2$ and dash-doted lines are for $w_m = 1/3$. The dependence of $\hat{\Omega}_{\rm e}(z)$ (red) remains constant with $w_m$ compare to $\hat{\Omega}_{\rm m}(z)$ (blue).

units of km/sec. The theoretical distance moduli $\mu^t$ for the k-th supernova at a distance $z_k$ is given by

$$\mu^t(z) = 5\log\left[\frac{d_L(z)}{\rm Mpc}\right] + 25 \tag{5.10}$$

So, the $\chi^2$ function for the SNe is defined as

$$\chi^2_{\rm SNe}(\alpha,\beta,\bar{\lambda},w_{\rm m},w_{\rm e}) \equiv \sum_{k=1}^{n}\left(\frac{\mu^t(z_k)-\mu_k}{\sigma_k}\right)^2 \tag{5.11}$$

where $\mu_k$ is the observed distance moduli of the k-th supernova, with a standard deviation of $\sigma_k$ in its measurement, and $n = 580$.

### 5.2.2 Hubble expansion rate

For the Hubble parameter we use 13 available data, 11 comes from the table 2 of Stern et al. (2010) [19] and the 2 following data from Gaztanaga et al. 2010 [20]: $H(z = 0.24) = 79.69 \pm 2.32$ and $H(z = 0.43) = 86.45 \pm 3.27$ km/s/Mpc. For the present value of the Hubble parameter we take that reported by Riess et al 2011 [21] $H(z = 0) \equiv H_0 = 73.8 \pm 2.4$ km/s/Mpc. The $\chi^2$ function is defined as

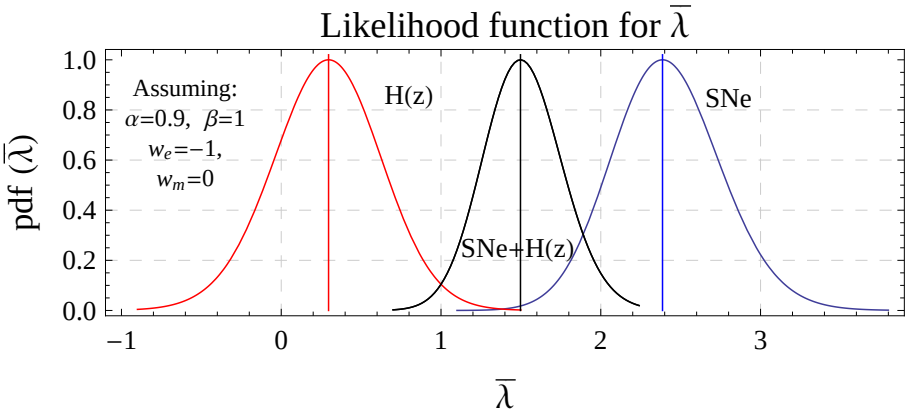


**Figure 7**. (Color on-line). Normalized probability density function **pdf** (or likelihood function) for the interaction coefficient $\bar{\lambda}$ assuming the values of ($\alpha = 0.9$, $\beta = 1$, $w_{\rm m} = 0$, $w_{\rm e} = -1$) and computed using the SNe (blue), $H(z)$ (red) and the joint SNe+$H(z)$ (black) data sets. The best estimated value for $\bar{\lambda}$ (the central value of the Gaussian) using the SNe+$H(z)$ data set is $\bar{\lambda} = 1.497 \pm 0.24$, with a $\chi^2_{\rm d.o.f.} = 1.3$. See table 1. So, it is found a non-vanishing value for the interaction coefficient, i.e., the interacting model is favored by the SNe+$H(z)$ observations. This model and the positive value of $\bar{\lambda}$ corresponds to an energy transfer from the cosmological constant ($w_{\rm e} = -1$) to the cold dark matter ($w_{\rm m} = 0$).

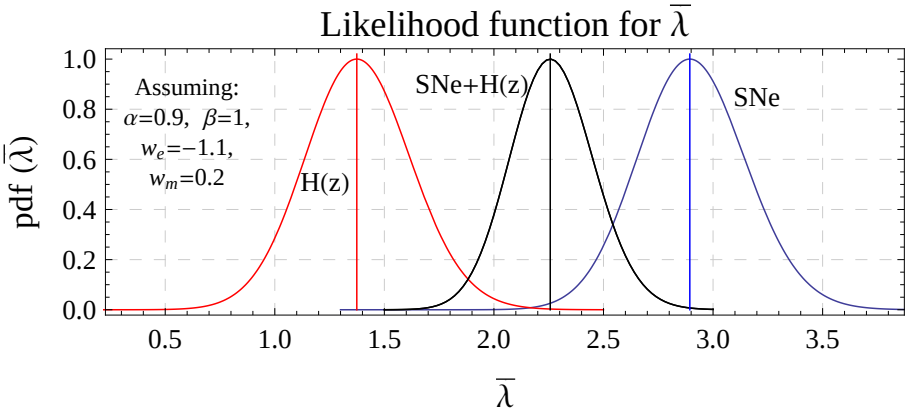


**Figure 8**. (Color on-line). Normalized likelihood function for the interaction coefficient $\bar{\lambda}$ assuming the values of ($\alpha = 0.9$, $\beta = 1$, $w_{\rm m} = 0.2$, $w_{\rm e} = -1.1$) and computed using the SNe (blue), $H(z)$ (red) and the joint SNe+$H(z)$ (black) data sets. The best estimated value for $\bar{\lambda}$ using the SNe+$H(z)$ data set is $\bar{\lambda} = 2.25 \pm 0.18$, with a $\chi^2_{\rm d.o.f.} = 1.29$. See table 1. It is found a non-vanishing value for the interaction coefficient. This model corresponds to a phantom dark energy ($w_{\rm e} = -1.1$) interacting with a warm dark matter ($w_{\rm m} = 0.2$). From the comparison of the value of $\chi^2_{\rm d.o.f.} = 1.29$ of this case with that of figure 7, where $\chi^2_{\rm d.o.f.} = 1.3$, we find that cosmological observations slightly prefer the interacting *phantom* dark energy to *warm* dark matter model instead of a cosmological constant interacting with a cold dark matter.

$$\chi^2_{\rm H}(\alpha, \beta, \bar{\lambda}, w_{\rm m}, w_{\rm e}) = \sum_i^{13} \left( \frac{H(z_i) - H_i^{\rm obs}}{\sigma_H} \right)^2 \tag{5.12}$$

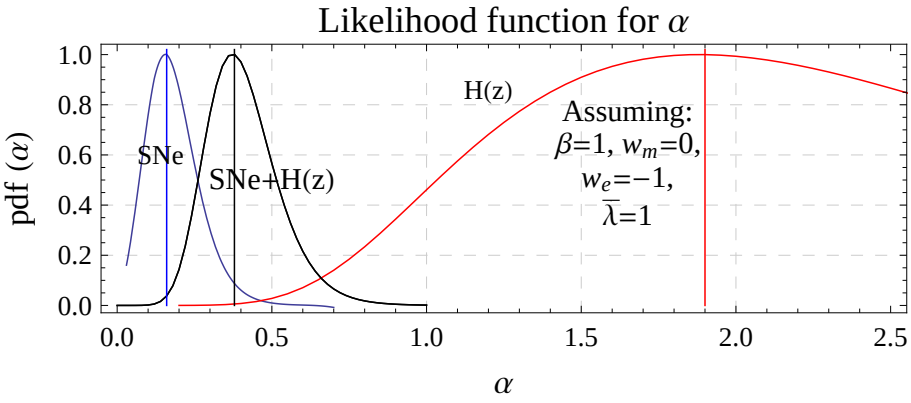


**Figure 9**. (Color on-line). Normalized likelihood function for the power $\alpha$ assuming the values of ($\beta = 1$, $\bar{\lambda} = 1$, $w_{\rm m} = 0$, $w_{\rm e} = -1$) and computed using the SNe (blue), $H(z)$ (red) and the joint SNe+$H(z)$ (black) data sets. The best estimated value for $\alpha$ using the SNe+$H(z)$ data set is $\alpha = 0.37^{+0.11}_{-0.10}$, with a $\chi^2_{\rm d.o.f.} = 1.29$. See table 1. This case corresponds to a cold dark matter interacting with a cosmological constant.

where $H(z_i)$ is the theoretical value predicted by the model and $H_i^{\rm obs}$ is the observed value.

## 6 Discussion and Conclusions

In order to shed some light on the coincidence problem we have explored a cosmological model composed by a dark matter fluid interacting with a dark energy fluid. Motivated for very recent investigations we have considered a warm dark matter. Since non-linear interactions represent a more physical plausible scenario for interacting fluid we studied an interaction which is given by the term $\lambda\rho_{\rm m}^{\alpha}\rho_{\rm e}^{\beta}$. We have found a general result which indicates that the positive critical points of the coincidence parameter $r = \rho_m/\rho_e$ exist if $w_e < -1$ independently of the interaction chosen and the particular EoS for the dark matter. We have considered from the beginning that the energy is transferred from dark energy to dark matter ($\lambda > 0$).

We performed an analytical analysis of the non-linear and coupled equations corresponding to the continuity equations for the dark matter and dark energy fluids. In particular we found the fixed points and their stability properties.

Using a high precision numerical method we solved these equations and were able not only to confirm with high accuracy the analytical results but also to extend the solutions beyond the validity regions of the analytical analysis.

The combined method described above allowed us to compute, in the densities space $(\rho_m, \rho_e)$, the behavior of the fixed points in terms of the parameters $\lambda, \alpha, \beta, w_{\rm m}$ and $w_{\rm e}$. Closed orbits were found for $w_e < -1.1$ and $\alpha = \beta = 1$. If $\alpha$ or $\beta$ or both of them are different from the unity, this closed orbits transform into spiral trajectories, evolving towards the origin for $\alpha < 1$ and $\beta = 1$, and away for the fixed point $\alpha = 1$ and $\beta > 1$. This analysis allowed to constrain the parameters in order to have physically reasonable scenarios, that is accelerated expansion in the late time phase of the cosmic evolution and far future evolution with finite DM and DE densities, which corresponds to spiral trajectories propagating from the fixed points.

The knowledge of these stability regions was used to fit with remarkable goodness the observational data to the physical model proposed in this paper.

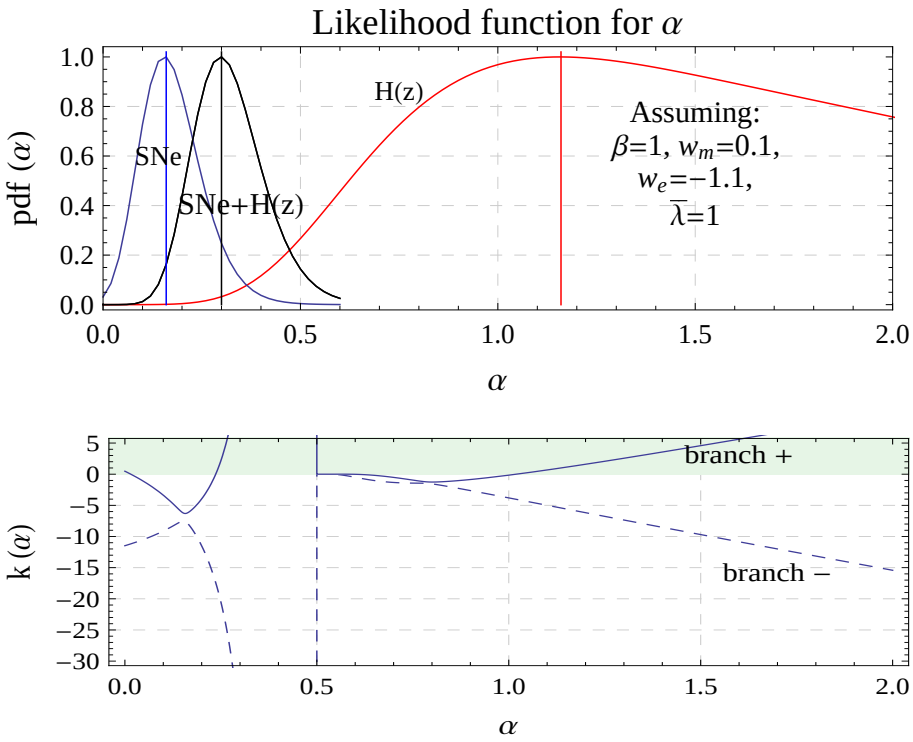


**Figure 10**. (Color on-line). The upper panel shows the normalized likelihood function for the power $\alpha$ assuming the values of ($\beta = 1$, $\bar{\lambda} = 1$, $w_{\rm m} = 0.1$, $w_{\rm e} = -1.1$) and computed using the SNe (blue), $H(z)$ (red) and the joint SNe+$H(z)$ (black) data sets. The best estimated value for $\alpha$ using the SNe+$H(z)$ data set is $\alpha = 0.30^{+0.09}_{-0.08}$, with a $\chi^2_{\rm d.o.f.} = 1.23$. See table 1. This case corresponds to a phantom dark energy interacting with a warm dark matter. The lower panel shows the values for $\alpha$ corresponding to *stable* solutions for $k(\alpha)$ [see eq. (3.18)], i.e., the regions where the solutions $k$ of the characteristic equation (3.18) are *negatives* in function of $\alpha$ and the given values of $(\beta, \bar{\lambda}, w_{\rm m}, w_{\rm e})$. The continuous and dashed plots correspond to the positive and negative branches of the solution of the quadratic equation (3.18) respectively.

Within this stability regions, the parameters $(\lambda, \alpha, \beta, w_{\rm m}, w_{\rm e})$ were estimated through the cosmological observations of the Union 2.1 type Ia supernovae data set and the Hubble parameter $H(z)$ at different redshift, that measure the late time expansion history of the Universe. We estimated $w_{\rm m}$ and $w_{\rm e}$ to explore the nature of these fluids in the context of this model. To compute the estimations of each of the five parameters, we assumed particular values for the other four. A summary of these results and assumptions are shown on table 1 and figures 7 to 14.

For the interacting coefficient $\lambda$, we defined a dimensionless $\bar{\lambda}$ for convenience. Using the cosmological observations it is found a non-vanishing positive value for $\bar{\lambda}$ with about 99.9% ($4\sigma$) of confidence level, indicating that the data prefer the interacting model instead of the non-interacting one, and that the energy transfer is from the dark energy (as cosmological constant) to the cold dark matter, for the assumed values of ($\alpha = 0.9, \beta = 1$). The same results are obtained when is assumed a *phantom* dark energy interacting with a *warm* dark matter, however, according to the values of $\chi^2$ in both case, the "phantom dark energy – warm dark matter" model fits better the data than the "cosmological constant – cold dark

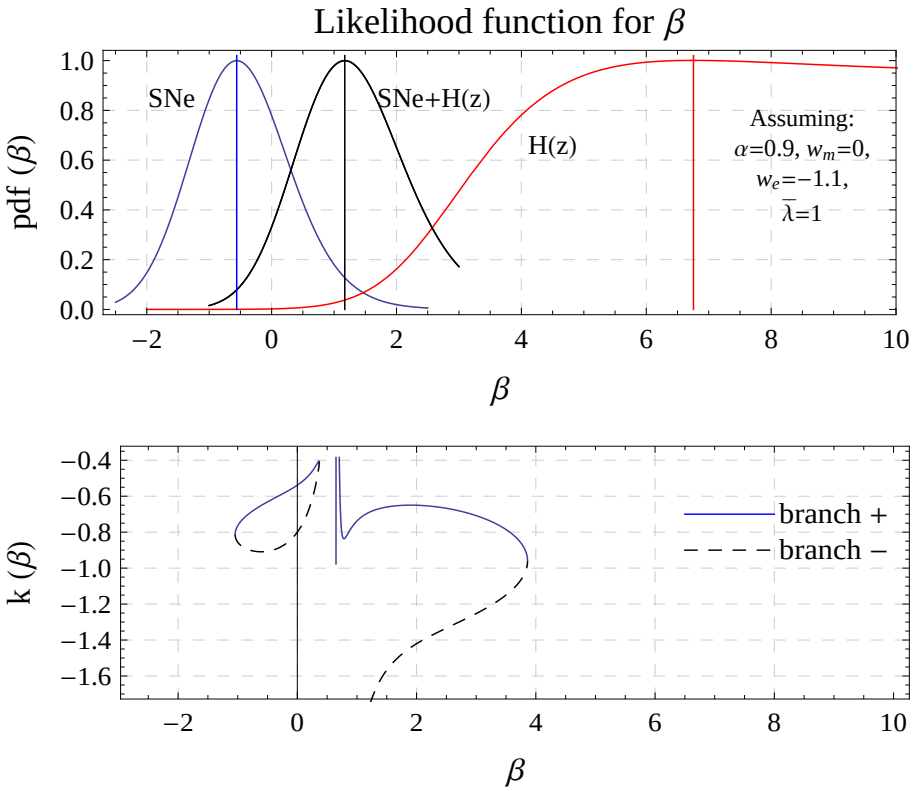


**Figure 11**. (Color on-line). The upper panel shows the normalized likelihood function for the power $\beta$ assuming the values of ($\alpha = 0.9$, $\bar{\lambda} = 1$, $w_{\rm m} = 0$, $w_{\rm e} = -1.1$) and computed using the SNe (blue), $H(z)$ (red) and the joint SNe+$H(z)$ (black) data sets. The best estimated value for $\beta$ using the SNe+$H(z)$ data set is $\beta = 1.171 \pm 0.8$, with a $\chi^2_{\rm d.o.f.} = 1.22$. See table 1. This case corresponds to a phantom dark energy interacting with a cold dark matter. The lower panel shows the values for $\beta$ corresponding to *stable* solutions for $k(\alpha)$ [see eq. (3.18)], where we have assumed the same values of ($\alpha$, $\bar{\lambda}$, $w_{\rm m}$, $w_{\rm e}$) as above. The continuous and dashed plots correspond to the positive and negative branches of the solution of the quadratic equation (3.18) respectively. The stable region for both branches are quite particular and narrow, however, the likelihood function for $\beta$ using SNe+$H(z)$ lies in this stable region.

matter" model.

For the power $\alpha$ of the dark matter density, we found that $\alpha > 0$ with about 99% of confidence level using the SNe+$H(z)$ dataset, indicating an interacting term of the form $\rho_{\rm e}\rho_{\rm m}^{\alpha}$, for the assumed values of ($\lambda = 1, \beta = 1$). This result is the same when we assume ($w_{\rm m} = -0, w_{\rm e} = -1$) or ($w_{\rm m} = -0.1, w_{\rm e} = -1.1$), however, the best fit to data is for the case of a phantom dark energy interacting with a warm dark matter.

For the power $\beta$ of the dark energy density, we found that $\beta > 0$ with about 68.3% ($1\sigma$) of confidence level using the SNe+$H(z)$ dataset, suggesting an interacting term of the form $\lambda\rho_{\rm e}^{\beta}\rho_{\rm m}^{\alpha}$, for the assumed values of ($\lambda = 1, \alpha = 0.9, w_{\rm m} = 0, w_{\rm e} = 1.1$). This case corresponds to a phantom dark energy interacting with a cold dark matter.

For the barotropic index $w_{\rm m}$ of the dark matter EoS, we found that the best estimated value is negative ($w_{\rm m} = -0.06 \pm 0.03$), when using the SNe+$H(z)$ and assuming ($\alpha = 1, \beta = 1, \lambda = 1, w_{\rm e} = -1.1$). When we impose the restriction $w_{\rm m} \geq 0$ we simply obtain $w_{\rm m} = 0.0$.

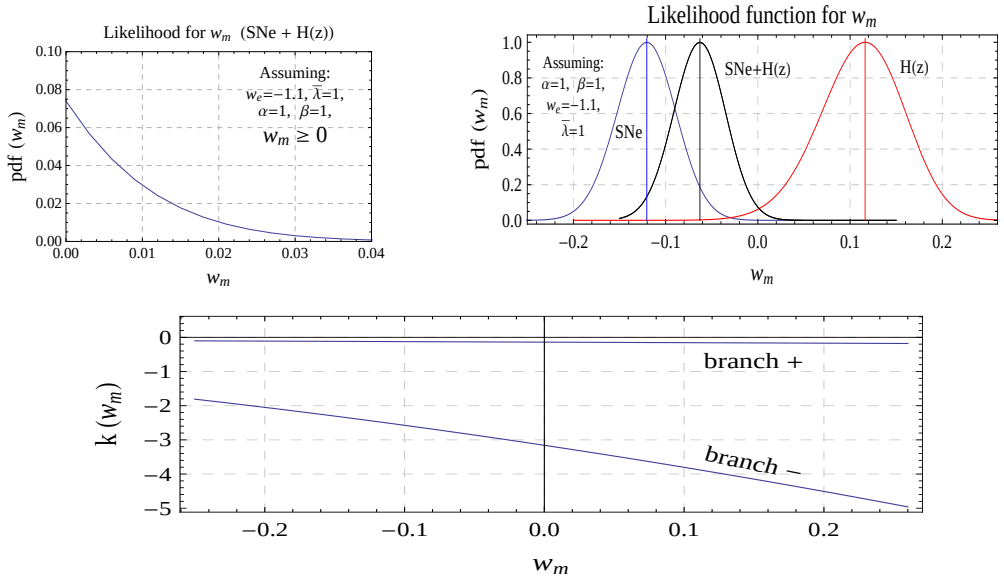


**Figure 12**. (Color on-line). The upper left panel shows the normalized likelihood function for the barotropic index $w_{\rm m}$ for the dark matter, assuming the values of ($\alpha = 1$, $\beta = 1$, $\bar{\lambda} = 1$, $w_{\rm e} = -1.1$) and the restriction $w_{\rm m} \geq 0$. The upper right panel shows the likelihood function for $w_{\rm m}$ computed without assume any restriction on the value of $w_{\rm m}$. The lower panel shows the values for $w_{\rm m}$ corresponding to *stable* solutions for $k(w_{\rm m})$ [see eq. (3.18)] where we have assumed the same values of ($\alpha$, $\beta$, $\bar{\lambda}$, $w_{\rm e}$) as above. The likelihood function of SNe $+H(z)$ lies in the the stable region for both branches.

And for the barotropic index $w_{\rm e}$ of the dark energy EoS, we found that it is constrained with 68.3% ($1\sigma$) of confidence level to $-1.32 < w_{\rm e} < -1.26$ and $-1.45 < w_{\rm e} < -1.39$, when it is assumed a cold and warm dark matter respectively, using the SNe+$H(z)$ dataset, that is clearly in the phantom regime for the dark energy.

On the other hand, from the value of $\chi^2_{\rm d.o.f.}$ seen as a measure of the goodness-of-fit to data, we find that from the cases studied in the present work, the best fit to the cosmological observations is obtained for the case with $\chi^2_{\rm d.o.f.} = 1.10$ (see table 1) that corresponds to a phantom dark energy ($w_{\rm e} = -1.4$) interacting with a warm dark matter ($w_{\rm m} = 0.1$), where the energy transfer comes from the dark energy to the dark matter ($\bar{\lambda} = 1$) and with an interacting term with the simple form "$\rho_{\rm m}\rho_{\rm e}$".

In summary, the non linear interaction chosen in this work leads to plausible scenarios that can alleviate the coincidence problem. The stable fixed points represent universes which end in a dark sector with non zero and finite energy densities in both fluids, despite the phantom behavior of the dark energy fluid. Finally, an interacting dark sector with a phantom like dark energy and warm dark matter fluid is well supported from cosmological observations.

## Acknowledgments

This work was supported by CONICYT through Grant FONDECYT N$^o$ Y1110840 (NC). GP was partially supported by DICYT-USACH Grant No 041231PA. A. A. acknowledges the very kind hospitality of Profs. G. P. and N. C. and the Departamento de Física of the Universidad de Santiago de Chile where a substantial part of the work was done.

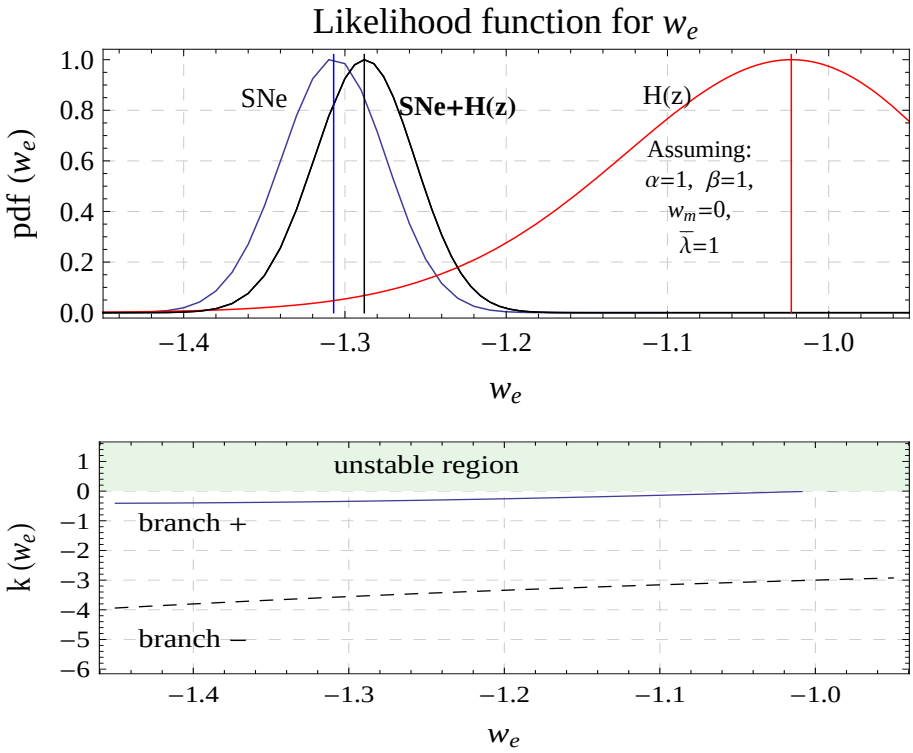


**Figure 13**. (Color on-line). The upper panel shows the normalized likelihood function for the barotropic index $w_{\rm e}$ for the dark energy, assuming the values of ($\alpha = 1$, $\beta = 1$, $\bar{\lambda} = 1$, $w_{\rm m} = 0$). The best estimated value for $w_{\rm e}$ using the SNe+$H(z)$ data set is $w_{\rm e} = -1.28 \pm 0.03$ with a $\chi^2_{\rm d.o.f.} = 1.14$. This case corresponds to a phantom dark energy fluid interacting with the cold dark matter. The lower panel shows the values for $w_{\rm e}$ corresponding to *stable* solutions for $k(w_{\rm e})$, where we have assumed the same values of ($\alpha$, $\beta$, $\bar{\lambda}$, $w_{\rm m}$) as above. The likelihood function of SNe $+H(z)$ lies in the the stable region for both branches.

## References


[1] A. G. Riess et al. [Supernova Search Team Collaboration], Astron. J. 116 (1998) 1009; S. Perlmutter et al. [Supernova Cosmology Project Collaboration], Astrophys. J. 517 (1999) 565; W. J. Percival *et al.* [The 2dFGRS Collaboration], Mon. Not. Roy. Astron. Soc. 327 (2001) 1297; P. Astier *et al.*, [astro-ph/0510447]; A.G.Riess et al. [Supernova Search Team Collaboration], Astrophys. J.607, 665 (2004).

[2] W. J. Percival *et al.* [The 2dFGRS Collaboration], Mon. Not. Roy. Astron. Soc. 327, 1297 (2001); M. Tegmark *et al.* [SDSS Collaboration], Phys. Rev. D 69 (2004) 103501; U. Seljak *et al.* [SDSS Collaboration], Phys. Rev. D 71 (2005) 103515.

[3] D. N. Spergel et al., [astro-ph/0603449]; A. C. S. Readhead et al., Astrophys. J. 609 (2004) 498; J. H. Goldstein et al., Astrophys. J. 599, 773 (2003) ; E. Komatsu *et al*, [WMAP Collaboration], Astrophys. J. Suppl. 189 (2009) 330-376 [astro- ph/0803.0547].

[4] D.J. Eisenstein *et al.* [SDSS Collaboration], Astrophys. J. 633 (2005) 560574, [astro-ph/0501171].

[5] B. Jain and A. Taylor, Phys. Rev. Lett. 91 (2003)141302, [astro-ph/0306046].

[6] P.J. Steinhardt, in Critical Problems in Physics, edited by V.L. Fitch and D.R. Marlow

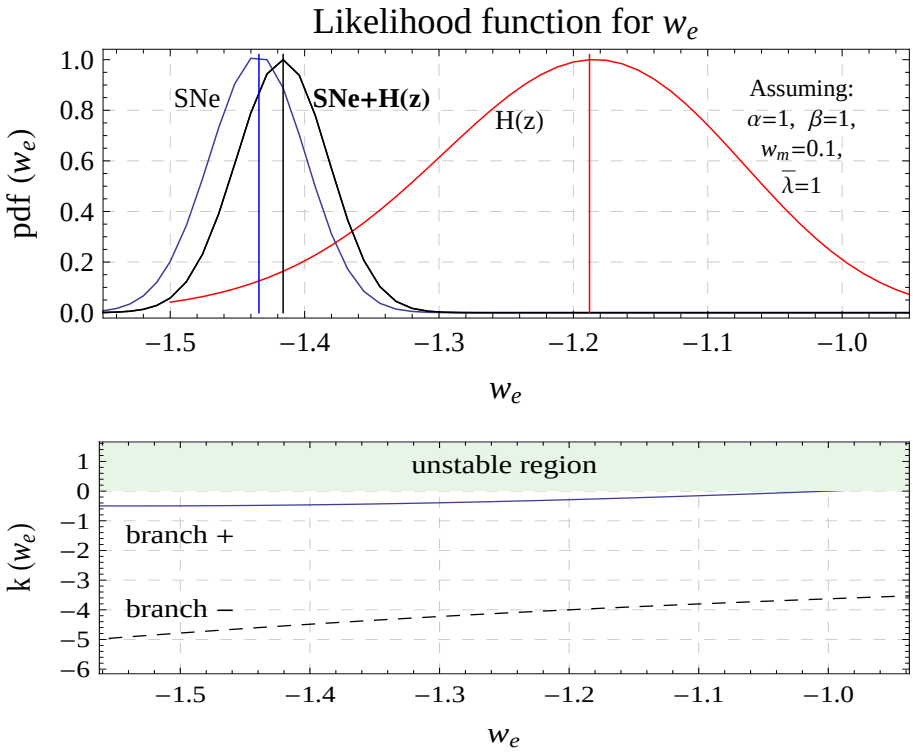


**Figure 14**. (Color on-line). The upper panel shows the normalized likelihood function for $w_{\rm e}$, assuming the values of ($\alpha = 1$, $\beta = 1$, $\bar{\lambda} = 1$, $w_{\rm m} = 0.1$). The best estimated value using the SNe+$H(z)$ data set is $w_{\rm e} = -1.416 \pm 0.03$ with a $\chi^2_{\rm d.o.f.} = 1.10$. This case corresponds to a phantom dark energy fluid interacting with a warm dark matter. The lower panel shows the values for $w_{\rm e}$ corresponding to *stable* solutions for $k(w_{\rm e})$, where we have assumed the same values of ($\alpha$, $\beta$, $\bar{\lambda}$, $w_{\rm m}$) as above. The likelihood function for SNe +$H(z)$ lie in the the stable region for both branches.

(Princeton University, Princeton, NJ, 1997); I. Zlatev, L.-M. Wang, and P. J. Steinhardt, Phys. Rev. Lett. 82, 896 (1999).

[7] L. Amendola, Phys. Rev. D 62, 043511 (2000); W. Zimdahl, D. Pavón and L.P. Chimento, Phys. Lett. B 521, 133 (2001); M. Gasperini, F. Piazza and G. Veneziano, Phys. Rev. D65, 023508 (2002); W. Zimdahl, Int. J. Mod. Phys. D 14, 2319 (2005); D. Pavón and W.Zimdahl, Phys. Lett. B 628, 206 (2005); G. Mangano, G. Miele and V. Pettorino, Mod. Phys. Lett.A 18, 831 2003); G. Farrar and P.J.E. Peebles, Astrophys. J. 604, 1 (2004); S. del Campo, R. Herrera and D. Pavón, Phys. Rev. D 70, 043540 (2004); R. Cai and A. Wang, J. Cosmol. Astropart. Phys.03, 002 (2005); Micheal S. Berger and H. Shojaei, Phys. Rev. D 73, 083528 (2006); Bo Hu and Y. Ling, Phys. Rev. D 73, 123510 (2006); Hui Li, Z. Guo and Y. Zhang, Int. J. Mod. Phys. D 15, 869 (2006); A. P. Billyard and A. A. Coley, Phys. Rev. D 61, 083503 (2000); M. Szydlowski, Phys. Lett. B 632, 1 (2006); M. Szydlowski, T. Stachowiak and R. Wojtak, Phys. Rev. D 73, 063516 (2006); L. P. Chimento, A. S. Jakubi, D. Pavón and W. Zimdahl, Phys. Rev.D 67, 083513 (2003); L. P. Chimento and D. Pavón, Phys. Rev.D 73, 063511 (2006); G. Olivares, F. Atrio-Barandela and D. Pavón, [gr-qc/0601086]; L. Amendola, G. Camargo Campos and R. Rosenfeld, [gr-qc/061006].

[8] R. G. Cai and A. Wang, *Cosmology with interaction between phantom dark energy and dark matter and the coincidence problem*, JCAP **0503** (2005) 002 [hep-th/0411025v4]; W. Zimdahl and D. Pavón, *Scaling Cosmology*, Gen. Rel. Grav. **35** (2003) 413-422 [astro-ph/0210484].

[9] Y. Ma, Y. Gong, and X. Chen, *Couplings between holographic dark energy and dark matter*, Eur. Phys. J. C **69** (2010) 509-519 [astro-ph.CO/0901.1215].

[10] G. Mangano, G. Miele and V. Pettorino, *Coupled quintessence and the coincidence problem*, Mod. Phys. Lett. A **18** (2003) 831–842 [astro-ph/0212518].

[11] S. Z. W. Lip, *Interacting cosmological fluids and the coincidence problem*, Phys. Rev. D **83**, 023528 (2011), Phys. Rev. D **83**, (2011) 023528 [gr-qc/1009.4942].

[12] F.Arevalo, A. P. Ramos Bacalhau, W. Zimdahl, *Cosmological dynamics with non-linear interactions*, [astro-ph.COS/1112.5095].

[13] D. Pavón and B. Wang, *Le Châtelier–Braun principle in cosmological physics*, Gen. Rel. Grav. **41**, (2009) 1–5 [gr-qc/0712.0565].

[14] P. Colin, V. Avila-Reese, and O. Valenzuela, Astrophys. J. 542, 622 (2000), astro-ph/0004115; V. Avila-Reese, P. Colin, O. Valenzuela, E. D'Onghia, and C. Firmani, Astrophys. J. 559, 516 (2001), astro-ph/0010525; P. Bode, J. P. Ostriker, and N. Turok, Astrophys. J. 556, 93 (2001), astro-ph/0010389; A. Knebe, J. E. G. Devriendt, A. Mahmood, and J. Silk, Mon. Not. R. Astron. Soc. 329, 813 (2002), astro-ph/0105316; A. Knebe, J. E. G. Devriendt, B. K. Gibson, and J. Silk, Mon. Not. R. Astron. Soc. 345, 1285 (2003), astro-ph/0302443; A. R. Zentner and J. S. Bullock, Astrophys. J. 598, 49 (2003), astro-ph/0304292; A. V. Maccio and F. Fontanot, astro-ph/0910.2460; A. L.Serra, M. J. de Leon Dominguez Romero, [gr-qc/1103.5465]; S. Bharadwaj and S. Kar, Phys. Rev. D68, 023516 (2003); K. Y. Su and P. Chen, Phys. Rev. D79, 128301 (2009).

[15] H. J. de Vega and N.G. Sanchez, *Warm dark matter in the galaxies: theoretical and observational progresses. Highlights and conclusions of the chalonge meudon workshop 2011* [astro-ph/1109.3187].

[16] L. Elsgoltz, *Ecuaciones diferenciales y cálculo variacional*, Editorial Mir, Moscu. (1969).

[17] G. Palma and V. H. Cardenas, *Resonance enhancement of particle production during reheating*, Class. Quantum Grav. **18** (2001) 2233 [gr-qc/0012005].

[18] N. Suzuki et al. The Hubble Space Telescope Cluster Supernova Survey: V. Improving the Dark Energy Constraints Above $z > 1$ and Building an Early-Type-Hosted Supernova Sample. *Astrophys. J.*, 746:85, 2012.

[19] Daniel Stern, Raul Jimenez, Licia Verde, Marc Kamionkowski, and S. Adam Stanford. Cosmic Chronometers: Constraining the Equation of State of Dark Energy. I: H(z) Measurements. *JCAP*, 1002:008, 2010.

[20] Enrique Gaztanaga, Anna Cabre, and Lam Hui. Clustering of Luminous Red Galaxies IV: Baryon Acoustic Peak in the Line-of-Sight Direction and a Direct Measurement of H(z). *Mon.Not.Roy.Astron.Soc.*, 399:1663–1680, 2009.

[21] Adam G. Riess, Lucas Macri, Stefano Casertano, Hubert Lampeitl, Henry C. Ferguson, et al. A 3% Solution: Determination of the Hubble Constant with the Hubble Space Telescope and Wide Field Camera 3. *Astrophys.J.*, 730:119, 2011.